AIAA JOURNAL
Vol. 45, No. 7, July 2007

Characterization of a Direct-Current Glow Discharge Plasma Actuator in Low-Pressure Supersonic Flow

Jichul Shin,* V. Narayanaswamy,* Laxminarayan L. Raja,† and Noel T. Clemens‡
University of Texas at Austin, Austin, Texas, 78712

DOI: 10.2514/1.27197

An experimental study of a direct-current, nonequilibrium glow plasma discharge in the presence of a Mach 2.85 supersonic flow is presented. The discharge is generated with pinlike electrodes flush-mounted on a plane surface with sustaining currents between 25 to 300 mA. In the presence of a supersonic flow, two distinct discharge modes (diffuse and constricted) are observed depending on the flow and discharge operating conditions. The effect of the discharge on the flow ("plasma actuation") is characterized by the appearance of a weak shock wave in the vicinity of the discharge. The shock is observed at low powers (∼10 W) for the diffuse discharge mode but is absent for the higher power (∼100 W) constricted mode. High-speed laser schlieren imaging suggests that plasma actuation is rapid as it occurs on a time scale that is less than 220 μs. Rotational (gas) and vibrational temperature within the discharge are estimated by emission spectral line fits of N_2 and N_2^+ rovibronic bands near 365–395 nm. The electronic temperatures are estimated by using the Boltzmann plot method for Fe(I) atomic lines. Rotational temperatures are found to be high (∼1500 K) in the absence of a flow but drop sharply (∼500 K) in the presence of a supersonic flow for both the diffuse and constricted discharge modes. The vibrational and electronic temperatures are measured to be about 3000 K and 1.25 eV, respectively, and these temperatures are the same with and without flow. The gas temperature spatial profiles above the cathode surface are similar for the diffuse and constricted modes indicating that dilatational effects due to gas heating are similar. However, complete absence of flow actuation as indicated visually by the shock indicates that electrostatic forces may also play an important role in high-speed plasma-flow actuation phenomena. Analytical estimates using cathode sheath theory indicate that ion pressure within sheath can be significant, resulting in gas compression within sheath and a corresponding expansion above it. The expansion, in turn, may fully negate the dilatational effect in the constricted case resulting in an apparent absence of forcing in the constricted case.

I. Introduction

THERE is much recent interest in plasma-based localized aerodynamic flow actuation using single dielectric-barrier discharges (DBD) [1,2], direct-current (DC) glow discharges [3–5], DC filamentary discharges [6,7], and RF discharges [8]. The use of plasmas for flow-control applications is particularly promising owing to the potential for achieving high-bandwidth actuation without moving mechanical parts. Plasma actuation is achieved through one or more of three basic mechanisms: 1) rapid gas heating of the flow achieved by volumetric Joule heating (dilatation effect), 2) electrohydrodynamic (EHD) forcing by imparting directed momentum to the bulk flow using electrostatic force generated by interaction of charge particles with an external electric field, and 3) magnetohydrodynamic (MHD) forcing, which relies on the generation of a Lorentz force on the bulk flow owing to the interaction of electrical currents with an externally imposed magnetic field.

In low-speed flows at atmospheric pressures, DBD-type actuators with asymmetric electrode/dielectric configurations have been used successfully for aerodynamic flow-control applications. Owing to the current limiting behavior of dielectric covered electrodes, these actuators are characterized by pulsed operation with 1–10 kV applied voltages at frequencies of ∼10 kHz and low peak current densities (∼1 A/m^2) [9–11]. DBD discharges generate low (room) temperature plasmas and rely on the EHD forcing mechanism. The main weakness of DBD actuators is the relatively small actuation effect as characterized by the induced flow velocity. For example, Roth [2] and Leonov et al.[7] have estimated induced velocities of about 10 m/s and less, in DBDs. In particular, Leonov et al. [7] comment that induced flow velocities higher than about 10 m/s are not possible in practice because increased DBD current results in increased gas heating and surface heating rather than EHD forcing. Results from the numerical studies of Shyy et al. [12] support the preceding estimates; they found that the maximum induced flow speeds were about 15 m/s and the maximum effect was obtained at very low freestream velocity (∼2 m/s).

Dilatation effects produced by gas heating in DC discharge have been shown to be much more effective in supersonic flow actuation. For example, Menart et al. [3] have shown that a diffuse DC glow discharge with an input power of about 50 W in a streamwise electrode arrangement (with cathode upstream) can increase the surface pressure in the immediate vicinity of the cathode by about 10%. Surface pressure measurements [3] and global force measurements on plasma-actuated surfaces [13] showed a linear trend with input power. However, a glow discharge is subject to instabilities especially at high pressures and high-current conditions [14]. The effectiveness of a diffuse glow discharge is therefore limited to currents of a few hundreds of milliampere. At higher currents, the glow transitions to a thermal arc. The arc itself is quite effective in supersonic flow actuation, albeit at much higher power inputs than the glow. For certain conditions, such as those studies by Yano et al. [15], a DC glow discharge in the presence of a supersonic flow did not show any detectable actuation of the flow, reflecting the relatively weak forcing effects that are often realized with plasma actuators in supersonic flows.

Flow actuation by large power deposition using filamentary arcs has been explored by Leonov et al. [6]. They used an array of small radius electrodes with input currents as high as 1–5 A at input voltages of several kilovolts. The power input in these discharges is a

Received 16 August 2006; revision received 2 March 2007; accepted for publication 5 March 2007. Copyright © 2007 by the American Institute of Aeronautics and Astronautics, Inc. All rights reserved. Copies of this paper may be made for personal or internal use, on condition that the copier pay the $10.00 per-copy fee to the Copyright Clearance Center, Inc., 222 Rosewood Drive, Danvers, MA 01923; include the code 0001-1452/07 $10.00 in correspondence with the CCC.

*Graduate Student, Aerospace Engineering and Engineering Mechanics. AIAA Student Member.
†Associate Professor, Aerospace Engineering and Engineering Mechanics. AIAA Member.
‡Professor, Aerospace Engineering and Engineering Mechanics. AIAA Associate Fellow.

few kilowatts and is much higher than in glows. For these arc discharges, the static pressure over the wall surface in the immediate vicinity of the discharge was measured and static pressure increases owing to the plasma discharges were found to be insignificant [6]. Similar pressure measurements were conducted by Menart et al. [3] whose results provide the same conclusions. However, schlieren imaging showed generation of weak shock waves at the location of the arc discharge and the formation of a separation zone immediately downstream of the electrodes [7].

Because dilatation effect produced by gas heating is significant in a nonmagnetized DC discharge, gas temperature information in the discharge is of great interest. In recent work of Stanfield et al. [16], temperature measurements in a diffuse glow discharge using emission spectroscopy found peak rotational temperatures to be around 380 K at 50 mA current input. A spatial profile of the temperature perpendicular to the surface above the cathode showed that the temperature decreased sharply to near freestream values of about 45 K at an elevation of about 3 mm with the peak occurring just above the cathode. These results indicate that gas heating takes place in only a small portion of the glow plasma volume near the cathode. In a filamentary arc discharge, gas temperatures as high as 3000–5000 K were measured [7], which is an order of magnitude higher than the case with a diffuse glow discharge [16]. However, as discussed previously, flow actuation by arcs is not significantly greater than flow actuation by diffuse glows, despite the much greater power inputs. Magnetic fields can potentially be applied to increase the effectiveness of plasma discharge by imposing a Lorentz force on the ionized flow. The effect of Lorentz forcing of a supersonic flow by an imposed magnetic field was explored recently, but even in this situation dilatation effects due to gas heating was shown to be the primary mechanism of flow actuation [5].

Measurements of the gas temperature using optical emission spectroscopy are common in plasma applications. Several methods, such as the Boltzmann plot of spectral line intensities, are used to evaluate the rotational, vibrational, and electronic temperatures of atomic/molecular species. For air plasma, the rotational bands of N_2^+ first negative system or N_2 second positive system are often used to determine the gas temperature [17]. In an N_2 spectrum, line strengths are usually determined by fitting the measured spectra to synthetic spectra, rather than by using the Boltzmann plot, owing to the overlap of rotational lines [17,18]. For example, Chelouah et al. [19] provide a reasonably good estimate of temperature using N_2 and N_2^+ bands by this fitting procedure.

In this paper, we study the coupled interactions between a DC glow plasma discharge with pinlike electrodes mounted on a surface, and a Mach 2.85 aerodynamic flow. Flash-lamp schlieren and high-speed laser schlieren imaging is used to visualize flow actuation by the discharge. Electrical measurements, synchronized with imaging, provide correlation between discharge structure and flow actuation phenomena and time-resolved current-voltage behavior. Non-intrusive optical emission spectroscopy (OES) is used to provide quantitative measurements of the gas temperature, molecular species vibrational temperature, and atomic species electronic temperature. We report different stable glow mode operation of the discharge depending on the discharge conditions. We also find the plasma actuation is highly dependent on the discharge mode and we speculate on the role of electrostatic forcing in addition to gas heating in the overall plasma actuation phenomena. This study therefore provides more evidence on the importance of electrostatic forcing alluded to by others in the literature [20].

II. Experiment Setup

A. Wind Tunnel

The experimental work was conducted in a Mach 2.85 wind tunnel with a test section that has a cross-sectional area of 25 cm^2. For our experiments, a splitter plate was inserted which extended from the plenum section into the test section, (Fig. 1). The acrylic splitter plate was 6.0 mm thick and the discharge electrodes were installed about 25 mm upstream of the trailing edge. The tunnel was equipped with adjustable upper and lower test section walls, which enabled the

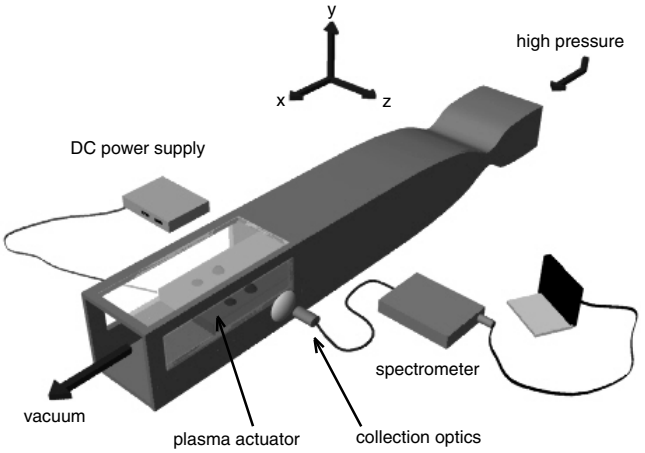

Fig. 1 Schematic of experiment setup for DC plasma-discharge supersonic flow actuation studies.

mean pressure gradient to be set. The tunnel was fed by a high-pressure tank and the air was discharged into a 1000 ft^3 vacuum tank. The vacuum tank was evacuated to a pressure of 5–10 torr by using a Stokes microvacuum pump (model 412H-11) and Roots Connersville rotary positive vacuum pump (RGS-HVB). The test section pressure was maintained in the range of 15–25 torr for all experimental runs. The freestream static temperature was about 110 K.

B. Plasma Discharge

A DC plasma was generated between two steel pinlike electrodes (diameter, 3/32 in.). The electrodes are flush-mounted on a ceramic plate (Macor or Mesco) that was inserted at the trailing edge of the splitter plate. The electrodes were oriented in the streamwise direction with one electrode upstream and the other downstream of it. The interelectrode distance measured between the electrode centers was 0.3 in. The electrodes are located about 4.5 in. downstream of the wind-tunnel nozzle exit and about 8 in. from the leading edge of the splitter plate.

Both cathode downstream and cathode upstream configurations were studied in this work. The discharge was generated by 1.2 kW high-voltage, high-current DC power supply (Spellman, SL2PN1200), which was rated to deliver a maximum current of 600 mA and a maximum voltage of 2 kV. A variable ballast resistor whose resistance ranged from 0 to 25 $k\Omega$ was connected in series to the ground electrode and was found necessary to provide control over the discharge operating regime. The discharge current was measured by measuring the voltage drop across an 11 Ω resistor connected in series to the discharge and was recorded using a data acquisition card (DAQcard-AI-16E-4). The transient discharge current measurement was synchronized with the high-speed laser schlieren imaging system.

C. Imaging

Flash-lamp schlieren imaging and laser schlieren imaging were used to visualize the flowfield structure in the supersonic flow. The flash lamp was pulsed at 60 Hz using a delay generator, and the pulse duration of about 2 μs was small enough to provide an instantaneous snapshot of the flow. The flow was imaged through acrylic windows on each side of the test section. The light was collimated and focused by 3 ft focal length concave mirrors. The schlieren images were captured using a Pulnix TM 6710 camera with a framing rate of 60 Hz, triggered internally, and had an exposure time of 16 ms. The images (512×480 pixel resolution) were acquired for 30 s once the tunnel was started. The optical setup for laser schlieren imaging was similar to that for flash-lamp schlieren, except that a steady-state helium-neon laser (5 mW) was used as the light source and a high-framing rate charge-coupled device (CCD) camera (Kodak Ektapro 4540mx) was used as the detector. The resolution of the CCD camera

was 256×256 pixels and the framing rate was 4.5 kHz (integration time of 222 μs). The start of the image acquisition was controlled using a delay generator and the images were acquired with an internal trigger.

D. Spectroscopy

Optical emission spectroscopy was used to obtain temperature information of the plasma discharge. The light emitted from the discharge was collected with a 1 in. focal length confocal lens (diameter, 1 in.) through a fused-silica side window and was focused onto a fiber optic cable with a 400 μm core. The fiber optic was connected to the entrance slit (5 μm slit width) of a 1/4 m imaging spectrometer (Spectra-Physics, MS260i). Collection optics (lens and fiber optic) were mounted on a translation stage to provide position control for the spatial temperature profile. No apertures were used for spectroscopic measurements. The nominal spectral resolution of the setup was 0.13 nm with a 1800 lines/mm grating. A study was performed to measure the spatial resolution of the optical setup by scanning a 25 μm pinhole back-illuminated by a flash lamp across the object plane. The spatial resolution was limited by the fiber optic cable core diameter and the magnification of the system, and was nominally 400 μm.

III. DC Plasma Discharge in Mach 2.85 Flow

The plasma discharge was ignited at interelectrode voltage drops between 500–1000 V depending on the test section pressure. The power supply provided the capability to establish a set-point current through the discharge by automatically varying the source voltage, and set-point currents were varied from 25 through 300 mA. Figure 2 shows laser schlieren images of 100 mA plasma discharges at different test section pressures in the absence of a flow. A diffuse luminous discharge is observed for pressures of 16.8, 20.32, and 25.4 torr. The luminosity is present only in the immediate vicinity of the cathode. As pressure increases at a fixed current of 100 mA, the volume of the luminous part of the discharge decreases. Further increase in pressure beyond a certain value extinguished the discharge, which indicates that higher voltages than could be delivered by the power supply were needed to sustain the plasma.

It is not uncommon to observe DC discharges with luminosity that is restricted to the cathode region. For example, in a certain range of pressures and in certain geometric configurations, a DC glow discharge may have a bright luminous cathode layer corresponding to the negative glow region, whereas the positive column remains less luminous or even dark [14]. The negative glow provides an indirect visual indication of the spatial extent of the sheath-bulk plasma-interface region. As the pressure increases and mean-free paths decrease, the characteristic dimension of the glow discharge decreases; this, in turn, is associated with a corresponding decrease in the spatial extent of the negative glow region. The observations in Fig. 2 are consistent with the preceding description of negative glow DC discharges, and thus provide some evidence that our discharge is in fact a nonequilibrium glow. It is useful to note that thermal arcs have vanishingly small sheaths and in general have a bright luminous positive column that extends from the cathode to the anode surfaces.

For a fixed pressure, the discharge current has a significant effect on its structure. Figure 3 shows luminosity images of the discharge with increasing currents in the absence of a flow at a fixed test section pressure of 15 torr. At 50 mA current, a luminous cathode layer (similar to Fig. 2) is observed with the positive column being dark (Fig. 3a). As the discharge current increases, the luminous cathode layer increases in size (Fig. 3b) and a further increase in current (Fig. 3c) results in a mode change where a diffuse discharge (with the luminous cathode layer) is replaced by a relatively constricted discharge. The constricted discharge mode is characterized by a luminous positive column region that spans the entire length between the cathode and the anode. A mode change of this nature in which diffuse glow discharge self-constricts above a certain threshold current is well documented in the literature (see [21], p. 474). It is also well established that the constricted mode is not necessarily a thermal arc because the discharge continues to be nonequilibrium in the

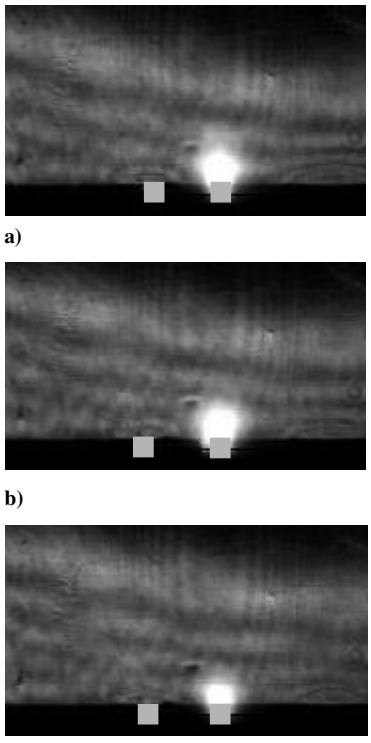

Fig. 2 Laser schlieren image of plasma discharge in absence of flow. Test section pressures a) 16.8 torr, b) 20.32 torr, and c) 25.4 torr. Electrode locations are shown as gray blocks with cathode on the right in each image.

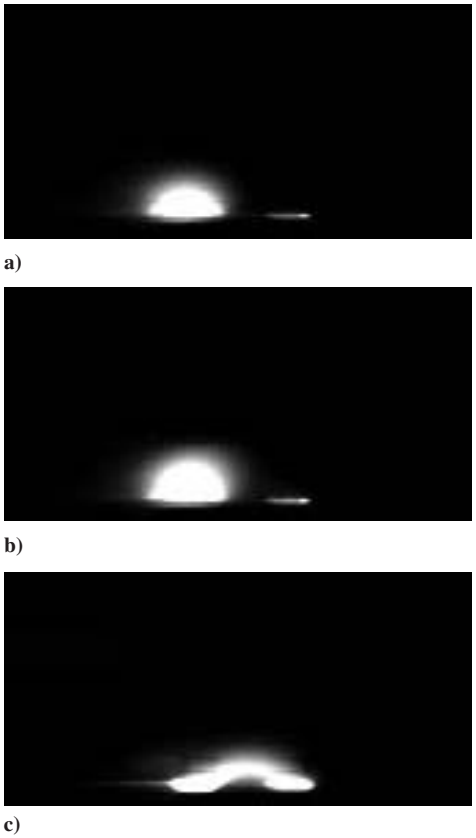

Fig. 3 Visible luminosity images of the discharge in absence of flow at a fixed pressure of 15 torr. Input currents are a) 50 mA, b) 150 mA, and c) 200 mA.

constricted mode, with the charge densities remaining well below typical densities for an arc. The constricted mode is therefore a nonequilibrium glow mode, albeit with higher charge densities than the diffuse glow mode. As will be discussed later, we also confirm the glow nature of the constricted mode by measuring highly disparate electrons, and heavy species temperatures. This mode change can therefore be characterized as a diffuse-to-constricted glow mode transition. At even higher current (>300 mA), secondary parasitic discharges occurred between the electrodes and the grounded test section walls, thereby establishing a practical upper limit to the currents we could run the discharge at. We also note that operation of the discharge does not cause a significant increase in the electrode/surface temperatures for both the diffuse and constricted discharge.

Figure 4 presents visible true color images of the discharge for different conditions in the presence of the supersonic flow. The flow is from the left to the right in each image (the cathode being on the left). Figure 4a is for a 100 mA discharge with a test section static pressure of 16 torr; Fig. 4b is for 150 mA and 25 torr, and Fig. 4c is for 150 mA and 15 torr. For the lower current and lower pressure case (Fig. 4a), the diffuse discharge with the luminous cathode layer (negative glow) is observed. The cathode layer has a distinct bluish color as seen in the image. Increasing the current and test section pressure to 150 mA and 25 torr, respectively, results in a mode where only the positive column in a relatively constricted discharge is visible (Fig. 4b). The positive column has a distinctive pink color indicating that different species are excited in the positive column compared with the luminous cathode layer in the case of the diffuse glow. For conditions with the same current (150 mA) as in Fig. 4b, but at lower pressure (15 torr), the discharge exhibits a bistable state in which both the diffuse mode (with a luminous cathode layer) and the constricted mode (with a luminous positive column) are possible. The discharge is observed to switch rapidly between these two modes, giving a visual (time-averaged) appearance that both a constricted positive column and a diffuse cathode layer occur simultaneously. Schlieren imaging (both flash-lamp and laser) applied to this bistable discharge shows individual images that resemble both Figs. 4a and 4b, and occasionally show images of the "mixed mode" with both constricted positive column and the diffuse cathode layer visible in the same image.

In all cases studied so far with supersonic flow, the overall discharge structure can be characterized by either one of the two modes (diffuse or constricted), with a third bistable state comprising a combination of the diffuse and constricted modes. It is convenient to classify the two modes as mode d (for diffuse glow discharge with the luminous cathode layer, as in Fig. 4a) and mode c (for constricted glow discharge with a luminous positive column, as in Fig. 4b), and a mode m (for bistable/mixed mode where both the cathode layer and the positive column are luminous in a time-averaged sense, Fig. 4c). Figure 5 provides a schematic illustration of the luminous regions corresponding to each mode.

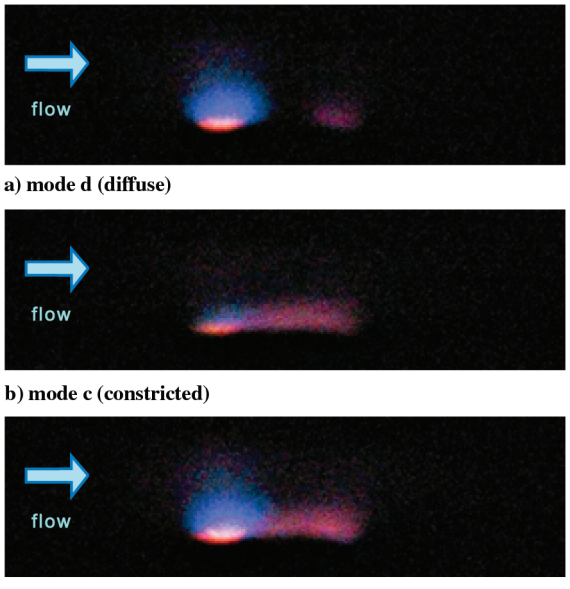

a) mode d (diffuse)

b) mode c (constricted)

c) mode m (mixed)

Fig. 4 Images of different discharge structures in the presence of flow.

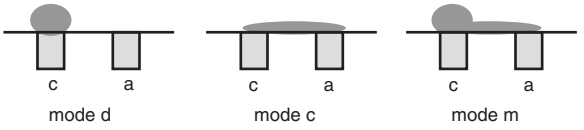

Fig. 5 Different modes of a DC discharge in a supersonic flow. Labels a and c denote the anode and cathode, respectively.

At pressures greater than about 25 torr, the discharge remains largely in the constricted mode c, whereas the discharge remains mostly diffuse (mode d) at lower pressures. Note that the size of the luminous region of the discharge does not change substantially either in the presence or absence of flow, as long as the discharge remained diffuse (mode d). It can be inferred from the preceding discussion that there is a definite pressure and current range over which the discharge remains diffuse and the current range is wider in the presence of flow due to aerodynamic stabilization [14].

Figure 6 shows representative time traces of the discharge current (I) and discharge voltage drop (V) transients during a short (2 s) period of a typical run. These transients are all for cases with the discharge in the presence of the supersonic flow and with a constant test section pressure of 16 torr. As shown in Fig. 6a, at a relatively low-power supply set-point current (75 mA), the discharge current and voltage drop across the discharge of about 0.5 kV were relatively steady. The discharge total resistivity under these conditions was therefore about 6.6 kΩ and the total power dissipated in the discharge was about 37 W. Schlieren images taken under these conditions confirm that the discharge was a diffuse mode d discharge. Figure 6b shows the case of a high set-point current of

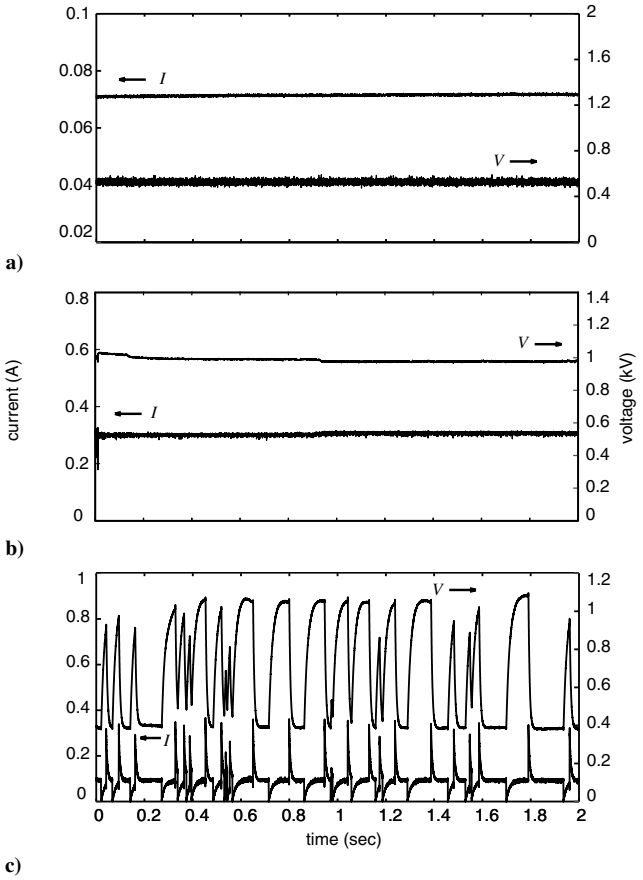

Fig. 6 Time records of current through and voltage drop across the DC discharges in the presence of a supersonic flow.

about 300 mA, and it is seen that a steady discharge corresponding to mode c is obtained. Here the discharge potential drop is about 1 kV and the discharge current is at the set-point current of 300 mA. The discharge resistivity in this constricted mode is about 3.3 kΩ, which is half the resistance of the diffuse mode. The total discharge power is, however, 300 W, which is about an order of magnitude greater than for the diffuse mode. For an intermediate power supply set-point current of 150 mA (Fig. 6c), the current-voltage transient reflects the bistable mode m discharge. The discharge is seen to abruptly transition from one mode to another with relatively long time periods on the order of hundreds of milliseconds, during which the discharge remains in a particular mode. It is clearly seen from the transients that during periods when the discharge remains at the set-point value of about 150 mA, the discharge voltage can be either close to 1 kV or around 0.4 kV, reflecting the high resistivity (mode d) and low resistivity (mode c) states, respectively. Immediately following a mode transition (as indicated by sharp spikes in the current transient, which occurs almost instantaneously on the transient time scale shown in the figure), the power supply responds by either increasing or decreasing the power supply voltage to maintain the current at the set-point value. The discharge voltage transient is determined by the response time of the power supply, which is on the order of 10 ms. These transient profiles are also consistent with the schlieren images of the mixed mode m discussed earlier. For these intermediate current conditions, individual schlieren images occur in one of mode d or mode c, and occasionally images having both a luminous cathode layer and positive column are observed as a consequence of a mode transition during the exposure time of the image. Regardless, it must be emphasized that the bistable mixed mode m at intermediate currents or pressures is a consequence of the nature of the power supply being used in our study, which tries to control the discharge current to a set-point value.

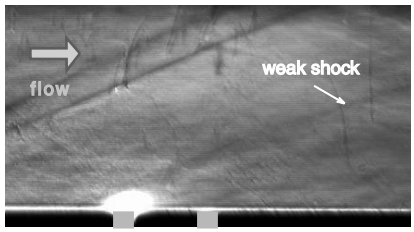

a)

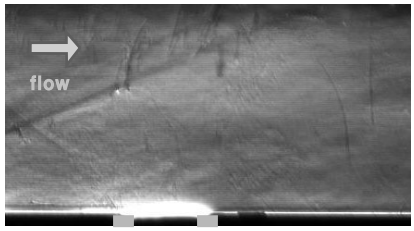

b)

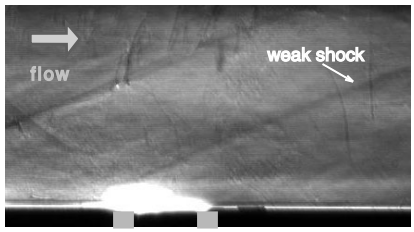

c)

Fig. 7 Flash-lamp schlieren imaging of flow interaction with the DC discharge. Weak shocks waves are observed in a) and c) but not in b).

IV. Plasma-Induced Flow Actuation

As we have seen, a DC glow plasma discharge can exhibit different modes in the presence of a supersonic flow depending on the discharge operating conditions and flow conditions. These discharge modes are also observed to have different interactions with the oncoming supersonic flow and consequently "actuate" the flow differently. Figure 7 shows three flash-lamp schlieren images of the flowfield structure of the Mach 2.85 supersonic flow in the presence of the DC glow discharge. The discharge current is 100 mA and pressure is 16 torr for Fig. 7a, 150 mA and 20 torr for Fig. 7b, and 150 mA and 16 torr for Fig. 7c. The discharge is in mode d in Fig. 7a, mode c in Fig. 7b, and mode m in Fig. 7c. For conditions corresponding to the diffuse discharge mode d (Fig. 7a), a perceptible effect of the discharge is observed on the flow through a weak oblique shock originating from the discharge region. The weak shock is completely absent in the case of a constricted mode c occurring at higher pressures and currents (Fig. 7b), indicating that the flow is unaffected by the discharge for this condition. This, however, does not preclude the possibility that the constricted mode c discharge does affect the pressure profiles in the near discharge region, although clearly the effect of this near discharge interaction is not evident in a far-field shock emerging from the discharge region. The schlieren image for the mixed mode m (Fig. 7c) also indicates the presence of a discharge-induced shock. For operating conditions corresponding to Fig. 7c, the shock is observed to be present for images with the discharge in mode d and absent for images with discharge in mode c, indicating that for all conditions it is necessary for the discharge to remain in the relatively low power (∼10 W) diffuse mode d rather than the higher power (∼100 W) constricted mode c to produce a visible effect of plasma-flow actuation. This observation is also consistent with surface pressure measurements of Kimmel et al. [5], who found that an increase of surface pressure just downstream of the cathode was much higher in the case of a low-current diffuse discharge compared with a more constricted discharge at higher currents. Our observations were highly repeatable and were confirmed through multiple experimental runs. Therefore, based on our schlieren imaging evidence of a shock emerging from the discharge region and consistent observations on the surface pressures measured by Kimmel et al. [5], we take the visible weak shock as measure of the effectiveness of plasma-flow interaction. We must also note that generation of discharge-induced flow actuation (discernible as shocks originating at the discharge location) has, however, been reported at much higher power (a few kilowatts) in filamentary arcs [22] where gas temperatures are high and dilatation effects are expected to be the only dominant mechanism of flow actuation in the absence of magnetic fields [5].

With high-speed laser schlieren, instantaneous snapshots of the discharge structure were recorded. For conditions corresponding to the bistable discharge mode m in Fig. 7c, the frame-by-frame schlieren images reveal that a discharge-induced shock appears within one frame after the discharge switches from the constricted mode c to the diffuse mode d. Similarly, the shock disappears within one frame after the discharge switches from diffuse mode d to constricted mode c. This indicates that the discharge mode switch occurs within the time period of 222 μs of each frame of the camera as was confirmed by the electrical characteristics of the mode m discharge in Fig. 7c. More important, these images show that flow actuation occurs on time scales shorter than the framing rate of the laser schlieren imaging, indicating that ∼100 μs flow actuation is indeed possible with plasma actuators. Clearly, either electrostatic forcing or rapid volumetric gas heating is responsible for the fast flow actuation phenomena. Also, the rapid time scales of actuation conclusively eliminate surface heating as the cause of flow actuation. More important, our results indicate that to obtain significant flow actuation in a surface localized DC glow discharge, the plasma must be operated in a relatively low-power diffuse mode d, which implies a limited set of pressure and discharge power conditions under which glow discharge based supersonic flow actuation is possible. Operating at higher powers resulted in a constricted discharge mode that was found to be relatively ineffective in flow actuation. For conditions under which the diffuse mode d glow discharge is not stable (higher pressures and higher powers), flow actuation is more effectively achieved at much higher powers (∼kWs) where filamentary arcs are generated [6].

V. Spectroscopic Measurement

As mentioned in the preceding section, in the absence of an external magnetic field, the actuation of supersonic flow in the DC glow discharge is achieved either by electrostatic forcing or dilatational effects owing to gas heating. To provide further insights into the potential role of dilatational effects, it is important to know the translational (gas) temperature of heavy species in the plasma. Because relatively high-pressure plasmas, such as the one investigated in this study, enable a fast rotational-translational energy transfer, the rotational temperature of the bulk gas can be assumed equal to the gas temperature. Nonintrusive optical emission spectroscopy of the discharge is commonly used to estimate the rotational temperature of molecular species in a discharge. In this paper, nitrogen band systems were studied because they can be easily identified in nitrogen carrying plasmas [23] and extensive reference data are available in the literature [17,24–27].

Figure 8 shows the emission spectrum of nitrogen rovibronic band systems in the wavelength range from 365 to 395 nm, in the Mach 2.85 supersonic flow. The spectrum is measured just above the cathode surface. The set-point current is 50 mA and the discharge is in the diffuse mode d. The N_2^+ first negative system $B^2\Sigma_u^+ \rightarrow X^2\Sigma_g^+$ at 391.44 nm (0–0) and N_2 second positive system $C^3\Pi_u \rightarrow B^3\Pi_g$ at 380.49 nm (0–2), 375.54 nm (1–3), and 371.05 nm (2–4) are observed. Rotational lines are much more distinguishable for the N_2^+ band compared with the N_2 bands. The corresponding emission spectra of the constricted mode c discharge at a current of 75 mA are shown in Fig. 9. Figure 9a is the spectrum measured above the cathode and Fig. 9b is measured just above the surface approximately midpoint between the anode and the cathode. Just above the cathode (Fig. 9a), emission from the N_2^+ (0–0) band is much stronger than that from the N_2 bands and the spectrum is similar to that taken at the same location for the diffuse mode d discharge (Fig. 8). The intensity of the N_2^+ band decreases significantly when measured in the positive column for the constricted mode c discharge (Fig. 9b). The differences in the relative intensities of the N_2^+ (0–0) band and the N_2 bands in different regions of the discharge are reflective of significant compositional differences in the different regions of the discharge; here, the positive column and the cathode layer. This is also responsible for the different luminous colors of the positive column and cathode layer as seen in the discharge structure images in Fig. 4. Note that the N_2 bands can be observed in most of the cases due to its large oscillator strength and large population in air [28].

Rotational temperatures were estimated by fitting synthetic spectra to the measured N_2 and N_2^+ rovibronic emission spectra. The N_2^+ rotational band was simulated assuming Hund's coupling case b and accounting for the intensity alternation owing to nuclear spin [29]. The N_2 rotational band was simulated using a representation intermediate between Hund's coupling cases a and b because the N_2 band conforms to Hund's case a at low rotational quantum numbers and case b at high rotational quantum numbers [29]. The resulting spectral lines were convolved with a Gaussian instrument broadening profile whose full-width at half-maximum was measured as 0.083 nm using an He-Ne laser. Doppler broadening was estimated to be three orders of magnitude smaller than instrument broadening. Stark broadening can be shown to be negligible under the relatively low electron density ($<10^{13}$ cm^{-3}) conditions expected in a glow discharge. Figure 10 shows spectral fits of N_2^+ and N_2 rotational bands of the 50 mA diffuse mode d discharge in the presence of a flow with test section static pressure of 16 torr. Almost all the peaks and valleys of the rotational lines match well in the N_2^+ fit. However in the N_2 fit, only the overall shape and line positions agree. This is because the gas temperature was low and hence the rotational lines were weak, and the N_2 lines were not resolved well with the spectrometer used [23]. In the procedure used, the generated synthetic spectra at certain temperatures were compared with measured spectra using a fixed line width and the error between two spectra was calculated. The error is obtained by considering running average of spectral line intensities near the wavelength of interest and it is represented as

$$\varepsilon_i = 11 \times I_i / \sum_{j=i-5}^{j=i+5} I_j$$

The errors were evaluated at various temperatures and the temperature estimate was taken at minimum error. Typical average error over a band is about 6–8%. For the spectrum shown in Fig. 10, rotational temperatures were estimated as 430 K for the N_2^+ fit and 400 K for the N_2 fit, respectively. Note that the freestream temperature of the Mach 2.85 supersonic flow is 110 K indicating that Joule (gas) heating of the flow is not negligible.

The estimates of rotational (gas) temperature at different currents are shown in Fig. 11 for a fixed test section static pressure of 16 torr. The solid line shows the temperature in the absence of a flow and the dotted line in the presence of a flow. The error bars represent 95% confidence intervals which are evaluated by assuming that statistical errors follow the Student t-distribution. The same error scheme will be used for temperature plots hereafter. The discharge structure was maintained in mode d for both cases. Currents beyond 125 mA are not included because higher currents result in mixed mode m or constricted mode c discharge structures. In the absence of a flow, temperatures were measured to be in the range of 1200–1800 K exhibiting a nearly monotonic increase with increasing current, except for the highest current of 125 mA, where the temperature drops slightly. In the presence of a flow, the temperatures are much lower, about 500 K, and show a slight increase with increasing current. The ambient gas temperature is at room temperature for cases without flow. For cases with supersonic flow, the freestream gas temperature drops significantly to about 110 K. Both the lower freestream temperature and convective effects in the flow explain the significantly lower gas temperatures of the discharge in the presence of a flow. However, the temperature increase caused by the discharge is still five times larger than the freestream temperature in the presence of a flow, indicating a significant gas heating by the plasma.

To provide insights into the volumetric extent of the gas heating, spatially resolved profiles of the measured rotational temperatures are shown in Fig. 12 for a diffuse mode d discharge (16 torr) and a constricted mode c discharge (30 torr) in the presence of the supersonic flow. These temperatures are again obtained using the spectral fitting of measured emission spectrum at different elevations (y direction; see Fig. 1) above the cathode. Note that the base elevation (0 mm) indicates where the spectral line intensity is detectable above the noise and this elevation is not necessarily the physical surface elevation. Also, the highest elevations for which temperature results are shown are the locations beyond which the spectral line intensities become too weak to estimate the temperature. The first data point is at 0.7 mm owing to the low signal below that elevation, and this location shows a temperature of about 800 K for

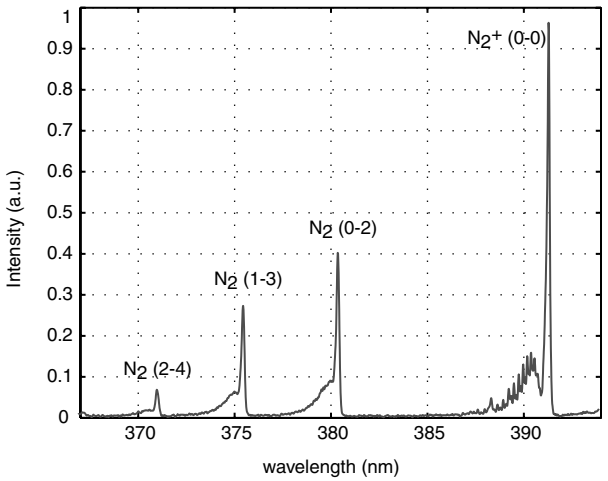

Fig. 8 Emission spectrum of air plasma in Mach 2.85 supersonic flow over a wavelength range of 365–395 nm.

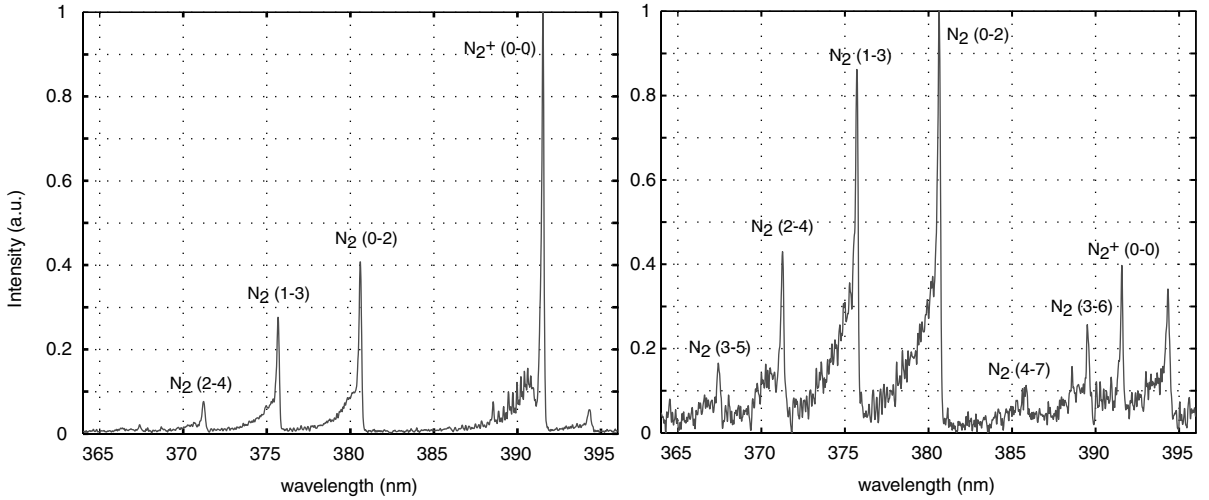

a) above cathode **b) midpoint between cathode and anode**

Fig. 9 Emission spectrum of air plasma in a Mach 2.85 supersonic flow in the wavelength range of 365–395 nm.

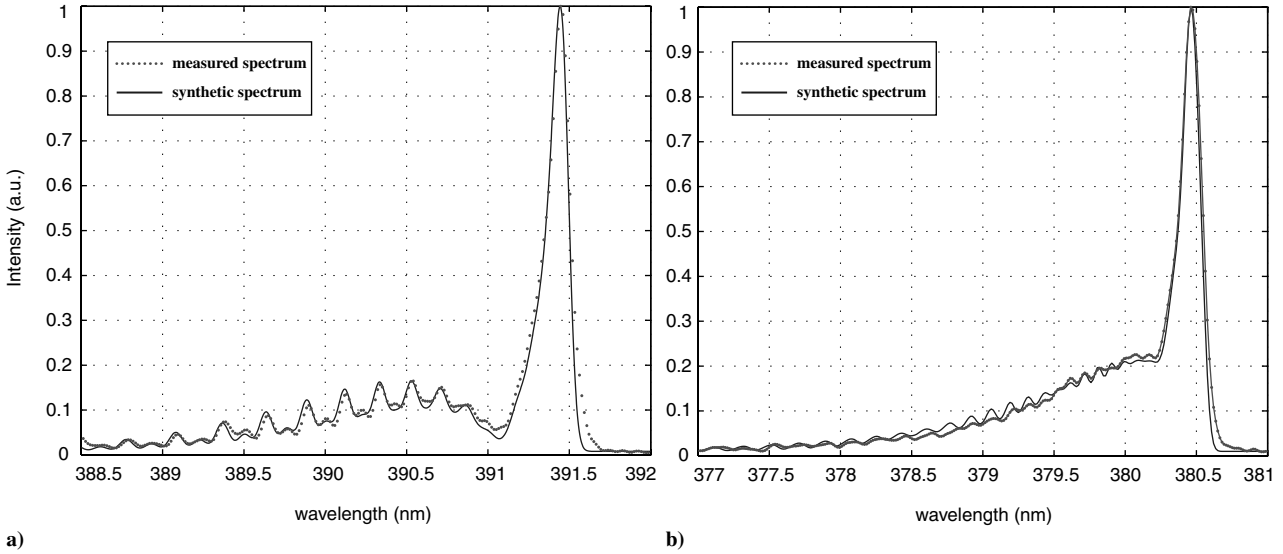

a) **b)**

Fig. 10 Spectral line fits of a) N_2^+ and b) N_2 rotational bands for a 50 mA diffuse mode d discharge in a Mach 2.85 supersonic flow.

both modes. At greater elevations above the cathode, the temperature drops to about 500 K at 2 mm for both modes. At elevations greater than 2 mm data are not available for the constricted mode, but data for the diffuse mode indicate that the temperature drops more gradually as shown in the figure. The gas temperature was also measured above the surface midway between the cathode and the anode for the constricted mode discharge and a similar profile is observed. Gas temperature measurements at the same midway location were not possible for the diffuse mode because of very weak emission at the location. Overall, results in Fig. 12 provide some insights into the dilatational effects due to gas heating in the diffuse mode and the constricted mode. Although the visible spatial extents of the discharge are much different for the diffuse mode and the constricted mode, the gas temperature profiles appear to be quite similar for the two modes. This similarity in the gas temperature spatial profiles provides some evidence that both the diffuse and the constricted modes produce similar dilatational effects on the flow.

Although rotational temperatures are nearly the same as the gas translational temperature, vibrational temperatures of molecular species can be significantly different from the translational temperature owing to much weaker vibrational-translational energy transfer. Once the rotational temperature was found by fitting the N_2 or N_2^+ rotational bands, band heads for (0–2), (1–3), and (2–4) vibrational transitions were matched by adjusting the vibrational temperature. Electronic moments and Frank–Condon factors for fitting different vibrational transitions were taken from the literature [25]. Figure 13 shows vibrational temperature profiles at different set-point currents. The solid line is for the case of the absence of flow and the dotted line is in the presence of the supersonic flow. The test

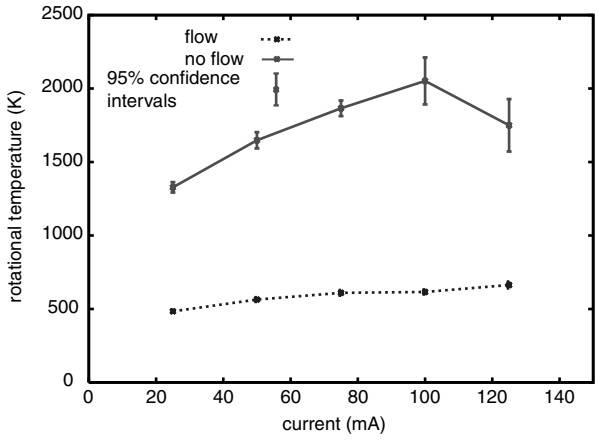

Fig. 11 Rotational (gas) temperatures as a function of the DC discharge current in a Mach 2.85 supersonic flow for a test section static pressure of 16 torr.

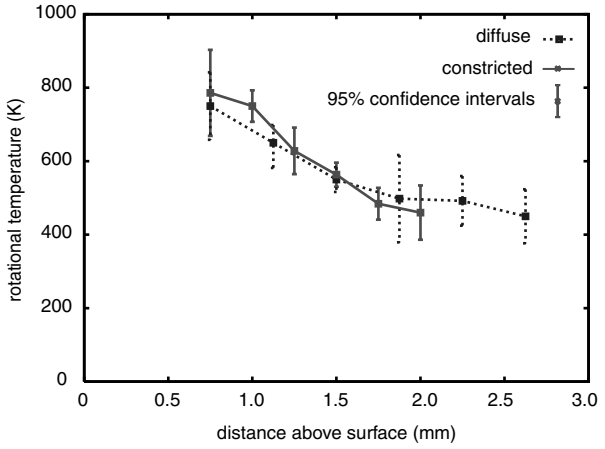

Fig. 12 Measured rotational temperatures as a function of the transverse distance above the cathode in a Mach 2.85 supersonic flow. Set-point current is 50 mA for both cases.

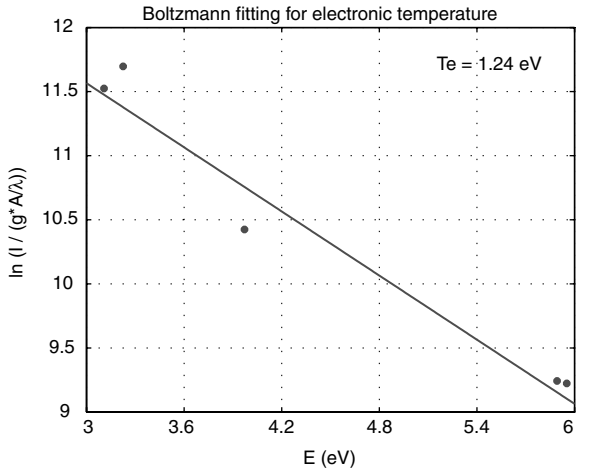

Fig. 14 Boltzmann plot of five different Fe(I) emission lines for estimation of electronic temperature.

section pressures are set at 15 torr to ensure that the discharge structures remain in the diffuse mode d discharge for both cases. Vibrational temperature estimates are about 2700 K for the no-flow case and slightly higher for the cases with the flow. Importantly, the vibrational temperatures are significantly higher than the rotational temperatures, which emphasizes the high degree of nonequilibrium in the discharge. It can be also observed from Fig. 13 that the vibrational temperature, unlike the rotational temperature, remains almost constant with increasing current.

Electronic populations were assumed to be in equilibrium with a single characteristic electron temperature. In the constricted mode c discharge, several atomic transition lines of Fe(I) were observed owing to erosion of the electrodes. In the case of the diffuse discharge, the metal lines are not distinguishable, presumably owing to much lower erosion rates in this mode. These lines were used to estimate the electron temperature by making a linear fit to the Boltzmann plot as shown in Fig. 14. The lowest electronic transitions are around 3 eV and the highest about 6 eV, providing a reasonable range of energies to characterize the electron energy distribution function. The electron temperature was found to be approximately 1.25 eV for all discharge conditions considered. The estimated electron temperature for the discharge in this report is quite similar to those reported in the literature [30,31].

VI. Discussion on DC Plasma Actuation Mechanism

As shown in the preceding section, significant gas heating is evident from our experimental results, which suggests that dilatational effects play an important role in flow actuation. The fact that both diffuse mode d and constricted mode c discharges have similar gas temperature spatial profiles (Fig. 12) implies that both modes produce similar dilatational effects on the flow. The dilatation effect due to gas heating is essentially an isotropic phenomena that causes a local high-pressure zone which imitates the presence of a surface bump. Consequently, if dilatation is the only mechanism by which plasma-flow actuation occurs, then one would expect the emergence of a weak shock from the discharge zone for both modes. However, the complete absence of any detectable flow actuation in the constricted mode c discharge suggests the possible importance of electrostatic forcing as an additional mechanism that influences the overall supersonic flow actuation phenomena.

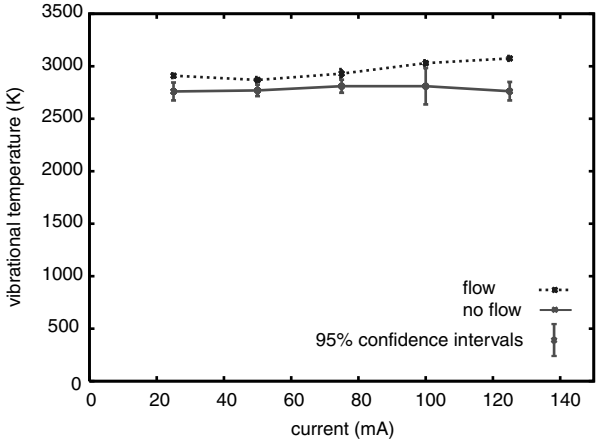

Fig. 13 Measured vibrational temperature in the presence of a Mach 2.85 supersonic flow. The discharge conditions are the same as in Fig. 12.

A rough estimate of electrostatic forcing effect for the diffuse mode d and constricted mode c discharge can be obtained using a collisional cathode sheath theory. The cathode directed drift motion of positive ions in the sheath can cause a compression of the gas within the sheath and a corresponding expansion of the gas above the sheath. We expect that the pressure increase within the sheath and expansion outside it must be a significant fraction of the total pressure if the electrostatic forcing effect is to be substantial. We assume a one-dimensional, planar, collisional DC sheath for simplicity and assume the Child's law sheath approximation of large cathode potential fall to be valid [32]. This approximation precludes the presence of all negatively charged particles in the sheath and only positive ions are accelerated through the cathode potential drop by mobility limited ion transport. Neglecting the contribution of secondary electron emission to the total discharge current, the number density of ions in the sheath is estimated as

$$n_i = \frac{J_0}{e\mu_i E} \tag{1}$$

where μ_i is the ion mobility which can be assumed a constant for a fixed pressure, E is the electric field in the sheath, and J_0 is the current density at the cathode. The sheath electric field is governed by the Poisson's equation as

$$\frac{dE}{dy} = \frac{e}{\varepsilon_0} n_i = \frac{J_0}{\varepsilon_0 \mu_i E} \tag{2}$$

where y is defined in the direction perpendicular to the electrode surface and the sheath edge plane, with $y = 0$ located at the sheath edge. Integrating once and assuming the electric field at the sheath edge is zero, we obtain an expression for the sheath electric field as

$$E = \left(\frac{2J_0}{\varepsilon_0 \mu_i} y\right)^{\frac{1}{2}} \tag{3}$$

Integrating again, we get an expression for the sheath thickness

$$t_s = \left(\frac{\varepsilon_0 \mu_i}{2J_0}\right)^{\frac{1}{3}} \left(\frac{3V_c}{2}\right)^{\frac{2}{3}} \quad (4)$$

which is a function of the cathode voltage drop V_c, the ion mobility, and the current density. The gas compression in the sheath is equivalent to the ion pressure rise in the sheath due to electrostatic forcing. Using the dominant terms in the ion momentum equation in the collisional sheath (ion pressure gradient and the electrostatic force), i.e., $\nabla p_i = en_i E$, the total ion pressure rise across the sheath is estimated as

$$\Delta p_i = \frac{J_0}{\mu_i} t_s \quad (5)$$

We can now make an estimate of the ion pressure (gas compression in the sheath) for both the diffuse mode d and constricted mode c discharges. A pressure of 16 torr with an ion mobility of 9×10^{-3} $m^2/V \cdot s$ (N_2^+ ion drifting in N_2) is assumed for both cases. For a diffuse mode d with low current, say $I = 50$ mA ($J_0 = 1.1 \times 10^4$ A/m^2) and a high cathode sheath voltage drop of $V_c = 1000$ V, the sheath thickness is predicted to be about 0.2 mm and the ion pressure rise is about 245 Pa (about 1.84 torr). On the other hand, for constricted mode c, with a higher current of say $I = 300$ mA ($J_0 = 6.7 \times 10^4$ A/m^2) and a lower voltage sheath voltage drop of $V_0 = 300$ V, the sheath thickness is about 0.05 mm and the ion pressure rise is about 367 Pa (2.76 torr). Clearly, the ion pressures rise and, hence, the gas pressure rise in the sheath in both the diffuse and constricted modes are comparable to the total pressure of 16 torr. The pressure rise, however, occurs in a much smaller cathode sheath thickness in the constricted case compared with the diffuse case. The corresponding expansion above the sheath occurs at distances much closer to the cathode surface in the constricted case compared with the diffuse case. We speculate that the expansion above the cathode sheath due to electrostatic forces in the sheath are responsible for either partly or fully negating the effect of dilatation. It is therefore plausible that in the constricted case, the expansion above the cathode sheath due to electrostatic forces almost fully negates the dilatation effect resulting in a complete absence of a shock and in the diffuse case, only a partial negation of the dilatation occurs resulting in the visible shock. A definitive discussion on the role of electrostatic forcing must, however, await more detailed experimental and theoretical investigations.

VII. Conclusions

DC glow plasma discharges were generated with pinlike electrodes in the presence of a Mach 2.85 supersonic flow. Different discharge structures like diffuse (mode d), constricted (mode c), and mixed (mode m) were observed exhibiting different interactions with the oncoming supersonic flow. The diffuse mode d discharge is produced when currents and test section pressures are low. Higher currents ($\gtrsim$150 mA) and higher pressures ($\gtrsim$25 Torr) drive the diffuse discharge into the constricted mode c discharge. The particular power supply we are using (current controlled) causes a bistable mixed mode at intermediate currents and pressures, where the discharge switches rapidly between the diffuse and constricted modes. In mode d, only the cathode layer with the negative glow is visible, whereas in mode c the positive column is also visible. Visible flow actuation was obtained for discharges in the diffuse mode d, as evidenced by the presence of a weak oblique shock originating at the cathode location on the surface. No such actuation was observed in the case of the constricted mode c discharge. High-speed laser schlieren imaging confirms that plasma actuation of the flow is achieved at high-bandwidth (of $\sim$100 μs or less actuation response time).

Rotational, vibrational, and electronic temperatures in the discharges were estimated by using optical emission spectroscopy. N_2^+ first negative and N_2 second positive rovibronic band systems were observed in both diffuse and constricted discharges. A significant decrease in the intensity of the N_2^+ system was observed in the positive column with constricted discharges, whereas the N_2 system was detected over the entire discharge volume. The rotational and vibrational temperature estimates were obtained by fitting synthetic spectra to the measured one. Gas temperatures (assumed to be equal to the N_2 and N_2^+ rotational temperatures) of a diffuse discharge in the absence of a flow were estimated around 1200–1800 K at set-point currents of 25–125 mA. In the presence of supersonic flow, gas temperature drops to near 500 K, remaining almost constant with increasing currents. Vibrational temperatures were measured to be as high as 3000 K, which is significantly higher than the rotational temperatures. Electronic temperature was found to be as high as 1.25 eV by Boltzmann fitting of Fe(I) atomic lines. The electronic temperature could only be estimated for the constricted mode because mode d did not exhibit sufficient emission from Fe(I). The disparate rotational, vibrational, and electronic temperatures confirm that both the diffuse and constricted mode discharges are glow discharges and not arcs. Spatially resolved gas temperature above the cathode surface showed very similar temperature profiles for the diffuse and constricted mode discharges resulting in very similar dilatational forcing effects for both discharge modes.

Finally, we discuss the role of electrostatic forcing in the cathode sheaths. A analytical model for collisional cathode sheaths confirms that significant gas pressure increases (compression) are obtained for both diffuse and constricted modes within the sheath. However, the cathode sheath thickness for the constricted mode is much smaller than the diffuse mode discharge. The compression within the sheath must be accompanied by a corresponding expansion outside the sheath, which can partially or fully negate the dilatational effect due to gas heating. We speculate that in the constricted case, the expansion above the sheath almost completely negates the dilatational forcing, resulting in the absence of a shock emerging from the discharge zone.

Acknowledgments

The authors would like to thank Philip Varghese for valuable discussions on the spectroscopic analysis. This study was supported by the United States Air Force Office of Scientific Research (Multidisciplinary University Research Initiative) under grant FA 9550-04-1-0387 with J. Tishkoff and J. Schmissuer as the program managers.

References

[1] Enloe, C. L., McLaughlin, T. E., VanDyken, R. D., Kachner, K. D., Jumper, E. J., and Corke, T. C., "Mechanisms and Responses of Single Dielectric Barrier Plasma Actuator: Plasma Morphology," *AIAA Journal*, Vol. 42, No. 3, 2004, pp. 589–594.

[2] Roth, J. R., "Aerodynamic Flow Acceleration Using Paraelectric and Peristaltic Electrohydrodynamic Effects of a One Atmosphere Uniform Glow Discharge Plasma," *Physics of Plasmas*, Vol. 10, No. 5, 2003, pp. 2117–2126.

[3] Menart, J., Shang, J., Kimmel, R., and Hayes, J., "Effects of Magnetic Fields on Plasmas Generated in a Mach 5 Wind Tunnel," AIAA Paper 2003-4165, June 2003.

[4] Menart, J., Handerson, S., Atzbach, C., Shang, J., Kimmel, R., and Hayes, J., "Study of Surface and Volumetric Heating Effects in a Mach 5 Flow," AIAA Paper 2004-2262, June 2004.

[5] Kimmel, R. L., Hayes, J. R., Menart, J. A., and Shang, J., "Effect of Surface Plasma Discharges on Boundary Layers at Mach 5," AIAA Paper 2004-509, Jan. 2004.

[6] Leonov, S., Bityurin, V., Savelkin, K., and Yarantsev, D., "Effect of Electrical Discharge on Separation Processes and Shocks Position in Supersonic Airflow," AIAA Paper 2002-0355, Jan. 2002.

[7] Leonov, S. B., Yarantsev, D. A., Gromov, V. G., and Kuriachy, A. P., "Mechanisms of Flow Control by Near-Surface Electrical Discharge Generation," *Vacuum*, Vol. 80, Nos. 11–12, 2006, pp. 1199–1205.

[8] Merriman, S., Ploenjes, E., Palm, P., and Adamovich, I. V., "Shock Wave Control by Nonequilibrium Plasmas in Cold Supersonic Gas Flows," *AIAA Journal*, Vol. 39, No. 8, 2001, pp. 1547–1552.

[9] Massines, F., Rahebi, A., Decomps, P., Ben Gadri, R., Segur, P., and Mayoux, C., "Experimental and Theoretical Study of a Glow Discharge at Atmospheric Pressure Controlled by Dielectric Barrier," *Journal of Applied Physics*, Vol. 83, No. 6, March 1998, pp. 2950–2957.

[10] Shin, J., and Raja, L. L., "Dynamics of Pulse Phenomena in Helium

Dielectric-Barrier Atmospheric-Pressure Glow Discharges," *Journal of Applied Physics*, Vol. 94, No. 12, Dec. 2003, pp. 7408–7415.
[11] Yuan, X., Shin, J., and Raja, L. L., "One-Dimensional Simulation of Multi Pulse Phenomena in Dielectric-Barrier Atmospheric-Pressure Glow Discharges," *Vacuum* (to be published).
[12] Shyy, W., Jayaraman, G., and Andersson, A., "Modeling of Glow Discharge-Induced Fluid Dynamics," *Journal of Applied Physics*, Vol. 92, No. 11, 2002, pp. 6434–6443.
[13] Menart, J., Stanfield, S., Shang, J., Kimmel, R., and Hayes, J., "Study of Plasma Electrode Arrangements for Optimum Lift in a Mach 5 Flow," AIAA Paper 2006-1172, Jan. 2006.
[14] Raizer, Y. P., *Gas Discharge Physics*, Springer, New York, 1991.
[15] Yano, R., Contini, V., Plönjes, E., Plam, P., Merriman, S., Aithal, S., Adamovich, I., Lempert, W., Subramaniam, V., and Rich, J. W., "Supersonic Nonequilibrium Plasma Wind-Tunnel Measurements of Shock Modification and Flow Visualization," *AIAA Journal*, Vol. 38, No. 10, 2000, pp. 1879–1888.
[16] Stanfield, S. A., Menart, J., Shang, J., Kimmel, R. L., and Hayes, J. R., "Application of a Spectroscopic Measuring Technique to Plasma Discharge in Hypersonic Flow," AIAA Paper 2006-559, Jan. 2006.
[17] Faure, G., and Shkol'nik, S. M., "Determination of Rotational and Vibrational Temperatures in a Discharge with Liquid Non-Metallic Electrodes in Air at Atmospheric Pressure," *Journal of Physics D: Applied Physics*, Vol. 31, No. 10, May 1998, pp. 1212–1218.
[18] Williamson, J. M., and DeJoseph, C. A., Jr., "Determination of Gas Temperature in an Open-Air Atmospheric Pressure Plasma Torch from Resolved Plasma Emission," *Journal of Applied Physics*, Vol. 93, No. 4, 2003, pp. 1893–1898.
[19] Chelouah, A., Marode, E., Hartmann, G., and Achat, S., "New Method for Temperature Evaluation in a Nitrogen Discharge," *Journal of Physics D: Applied Physics*, Vol. 27, No. 5, May 1994, pp. 940–945.
[20] Menier, E., Leger, L., Depussay, E., Lago, V., and Artana, G., "Effect of a DC Discharge on the Supersonic Rarefied Air Flow over a Flat Plate," *Journal of Physics D: Applied Physics*, Vol. 40, No. 3, Feb. 2007, pp. 695–701.
[21] Fridman, A., and Kennedy, L. A., *Plasma Physics and Engineering*, Taylor and Francis, Philadelphia, PA, 2004.
[22] Leonov, S., Bityurin, V., and Yarantsev, D., "Effect of Plasma Induced Separation," AIAA Paper 2003-3853, June 2003.
[23] Williamson, J. M., Bletzinger, P., and Ganguly, B. N., "Gas Temperature Determination in a N2/Ar Dielectric Barrier Discharge by Diode-Laser Absorption Spectroscopy and Resolved Plasma Emission," *Journal of Physics D: Applied Physics*, Vol. 37, No. 12, June 2004, pp. 1658–1663.
[24] Hartmann, G., and Johnson, P. C., "Measurements of Relative Transition Probabilities and the Variation of the Electronic Transition Moment for $N_2C^3\Pi_u$-$B^3\Pi_g$ Second Positive System," *Journal of Physics B: Atomic and Molecular Physics*, Vol. 11, No. 9, 1978, pp. 1597–1611.
[25] Nassar, H., Pellerin, S., Musiol, K., Martinie, O., Pellerin, N., and Cormier, J.-M., "N_2^+/N_2 Ratio and Temperature Measurements Based on the First Negative N_2^+ and Second Positive N_2 Overlapped Molecular Emission Spectra," *Journal of Physics D: Applied Physics*, Vol. 37, No. 14, July 2004, pp. 1904–1916.
[26] Laux, C. O., and Kruger, C. H., "Arrays of Radiative Transition Probabilities for the N_2 First and Second Positive, NO Beta and Gamma, N_2^+ First Negative, and O_2 Schumann–Runge Band Systems," *Journal of Quantitative Spectroscopy and Radiative Transfer*, Vol. 48, No. 1, 1992, pp. 9–24.
[27] Lofthus, A., and Krupenie, P. H., "Spectrum of Molecular Nitrogen," *Journal of Physical and Chemical Reference Data*, Vol. 6, No. 1, 1977, pp. 113–307.
[28] Phillips, D. M., "Determination of Gas Temperature from Unresolved Bands in the Spectrum from a Nitrogen Discharge," *Journal of Physics D: Applied Physics*, Vol. 8, No. 3, March 1975, pp. 507–521.
[29] Herzberg, G., *Molecular Spectra and Molecular Structure 1: Spectra of Diatomic Molecules*, Van Nostrand Reinhold, New York, 1962.
[30] Surzhikov, S. T., and Shang, J., "Two-Component Plasma Model for Two-Dimensional Glow Discharge in Magnetic Field," *Journal of Computational Physics*, Vol. 199, No. 2, Sept. 2004, pp. 437–464.
[31] Deconinck, T., Mahadevan, S., and Raja, L. L., "Self-Consistent Two-Dimensional Simulations of Glow Discharge Phenomena for High-Speed Flow Control," AIAA Paper 2006-372, Jan. 2006.
[32] Lieberman, M. A., and Lichtenberg, A. J., *Principles of Plasma Discharges and Materials Processing*, Wiley, New York, 1994.

N. Chokani
Associate Editor